Maladaptive Shifts in Life History in a Changing Environment

Olivier Cotto, Linnéa Sandell, Luis-Miguel Chevin, Ophélie Ronce

SPECIAL FEATURE ON MALADAPTATION

Maladaptive Shifts in Life History in a Changing Environment*

Olivier Cotto,[1,†,‡] Linnea Sandell,[2,3,†] Luis-Miguel Chevin,[1] and Ophélie Ronce[3,‡]

1. Centre d'Ecologie Fonctionnelle et Evolutive (CEFE), Centre National de la Recherche Scientifique (CNRS), Université de Montpellier, Université Paul Valéry Montpellier 3, École Pratique des Hautes Études (EPHE), Institut de Recherche pour le Développement (IRD), Montpellier, France; 2. Department of Zoology, University of British Columbia, Vancouver, British Columbia, Canada; 3. Institut des Sciences de l'Évolution, Université de Montpellier, CNRS, IRD, EPHE, Montpellier, France

Submitted March 12, 2018; Accepted September 11, 2018; Electronically published March 18, 2019

Online enhancements: appendix. *Dryad data:* https://dx.doi.org/10.5061/dryad.2g7g3dc.

ABSTRACT: Many species facing climate change have complex life cycles, with individuals in different stages differing in their sensitivity to a changing climate and their contribution to population growth. We use a quantitative genetics model to predict the dynamics of adaptation in a stage-structured population confronted with a steadily changing environment. Our model assumes that different optimal phenotypic values maximize different fitness components, consistent with many empirical observations. In a constant environment, the population evolves toward an equilibrium phenotype, which represents the best compromise given the trade-off between vital rates. In a changing environment, however, the mean phenotype in the population will lag behind this optimal compromise. We show that this lag may result in a shift along the trade-off between vital rates, with negative consequences for some fitness components but, less intuitively, improvements in some others. Complex eco-evolutionary dynamics can emerge in our model due to feedbacks between population demography and adaptation. Because of such feedback loops, selection may favor further shifts in life history in the same direction as those caused by maladaptive lags. These shifts in life history could be wrongly interpreted as adaptations to the new environment, while in reality they only reflect the inability of the population to adapt fast enough.

Keywords: life history, trade-off, maladaptation, changing environments.

Introduction

Natural selection acting on quantitative traits in the wild varies in direction, strength, variability, and sensitivity to environmental drivers, depending on the fitness component used to measure selection (Kingsolver and Diamond 2011; Siepielski et al. 2011, 2017). Relatively few studies have estimated selection gradients on the same trait using different fitness components. In 43% of those, the direction of selection reversed when considering the effect of the trait on survival or fecundity (compared with 57% for which the direction was the same; Kingsolver and Diamond 2011). Reviewing early evidence for opposite selection at different stages of life history, Schluter et al. (1991) concluded that conflicting selection pressures may be key to understanding both the evolution of phenotypes and the mechanisms of life-history trade-offs. Calls to unify selection and life-history theory have been repeated recently, motivated by empirical evidence that conflicting selection pressures on the same phenotypic traits across the life cycle may be critical to understanding adaptation to climate change in many plants and animals (Ehrlén and Münzbergová 2009; Mojica and Kelly 2010; Tarwater and Beissinger 2013; Vitasse 2013; Childs et al. 2016; Wadgymar et al. 2017). Interestingly, phenological traits appear to frequently be subject to such conflicting selection pressures. For instance, Wadgymar et al. (2017) found that the flowering date maximizing survival of the perennial plant *Boechera stricta* was later than the date maximizing fruit production. Conversely, earlier laying date is associated with increased survival but lower recruitment in the great tit *Parus major* (Childs et al. 2016). Understanding patterns of local adaptation to climatic gradients therefore requires integrating variation of selection across fitness components (Wadgymar et al. 2017). Our aim in this article is to advance our theoretical understanding of the consequences of such conflicting selection pressures for the dynamics of adaptation, life history, and demography of a population confronted with climate change.

Populations facing a changing environment, as occurs under climate change, must adapt fast enough to persist. Several theoretical models have formalized such demographic and evolutionary challenges and predicted the critical speed of environmental change above which the population is doomed (Lynch et al. 1991; Lynch and Lande 1993; Bürger and Lynch

* The Special Feature on Maladaptation is a product of a working group that convened in December 2015 and 2016 at McGill University's Gault Preserve and of a symposium held at the 2018 meeting of the American Society of Naturalists in Asilomar, California, inspired by the working group.

† These authors served as lead authors for this project and contributed equally.

‡ Corresponding authors; email: ophelie.ronce@umontpellier.fr, olivier.cotto2@gmail.com.

ORCIDs: Cotto, https://orcid.org/0000-0003-0737-5879.

Am. Nat. 2019. Vol. 194, pp. 000–000.
DOI: 10.1086/702716

1995; Lande and Shannon 1996; Willi and Hoffmann 2009; Gienapp 2013; for a very complete review, see Kopp and Matuszewski 2014). These quantitative genetics models assume that the contribution of an individual to the population growth rate depends on the match of its phenotype to some optimal phenotype. This optimal phenotype changes with the environment through time in a linear fashion, with a constant speed. Under the assumptions of these models, the strength of directional selection on the phenotype increases proportionally to the distance between the mean phenotype and the optimal phenotype (for alternative assumptions, see Osmond and Klausmeier 2017). Consider a population initially well adapted to its environment. As the optimum starts moving, selection is initially weak, the population evolves more slowly than the environment changes, and the lag between the mean and optimal phenotypes increases. Increasing lag results in stronger selection and faster evolution until the population reaches a dynamical equilibrium where it evolves as fast as the environment changes. The population then tracks the moving optimum with a constant lag, proportional to the speed of environmental change. This phenotypic mismatch is at the origin of a genetic load (referred to as an evolutionary load or lag load; Lande and Shannon 1996) depressing the mean population growth rate. When the equilibrium lag is too large to allow population growth, extinction cannot be avoided. Developments of this theory have explored in particular how this critical rate of environmental change was affected by phenotypic plasticity (Chevin et al. 2010; Nunney 2015), multivariate selection (Gomulkiewicz and Houle 2009; Chevin 2013), spatial heterogeneity of selection (Polechová et al. 2009; Aguilée et al. 2016), or combinations of these factors (Duputié et al. 2012).

Many species facing climate change have complex life cycles, with individuals in different stages differing in their sensitivity to a changing climate and their contribution to population growth (Crozier et al. 2008; Marshall et al. 2016). This complexity makes predictions about their joint adaptation and population dynamics nontrivial. Fortunately, sophisticated models combining quantitative genetics and demography are currently being developed, building on the foundational work of Lande (1982) and allowing much progress in this direction (e.g., Barfield et al. 2011; Engen et al. 2011; Childs et al. 2016; Coulson et al. 2017; Janeiro et al. 2017; Orive et al. 2017). Models of adaptation to a changing environment found that overlapping generations could slow down the evolutionary response, increase phenotypic lags, and decrease prospects of persistence (Zeineddine and Jansen 2009; Kuparinen et al. 2010; Cotto et al. 2017; Orive et al. 2017). Interestingly, these effects are predicted in the absence of any direct trade-off between survival and fecundity. The previous models indeed assume that selection acts on a single component of the life cycle (juvenile viability: Kuparinen et al. 2010; Orive et al. 2017; Cotto et al. 2017; fecundity: Zeineddine and Jansen 2009). Recently, Marshall et al. (2016) predicted that selection acting sequentially on several stages in the life cycle, with different sensitivities to environmental change, also increases adaptation lags and makes species with complex life cycles more prone to extinction in a changing environment. The model by Marshall et al. (2016) assumes nonoverlapping generations and partially correlated traits across life stages, being formally equivalent to a multivariate model of adaptation to a changing environment (e.g., as in Gomulkiewicz and Houle 2009; Duputié et al. 2012; Chevin 2013).

Another interesting property of complex life cycles is that individuals in different stages may have, on average, very different contributions to total population growth: the strength of selection on a phenotypic trait through its effect on some transition in the life cycle thus depends on how disturbance in this transition affects total fitness. The latter can be measured by demographic elasticities, well known to demographers (Caswell 2001). Cotto and Ronce (2014) showed that in changing environments, decline in the strength of selection with age should result in larger lags in adaptation for those traits that affect fitness late in life rather than early. Variation in maladaptation across stages modifies the life history, which may feed back on evolutionary responses through changes in demographic elasticities. As a result of these feedbacks, Cotto and Ronce (2014) found that when environmental change was fast, adaptation lags in older age classes kept increasing with time. This contrasts with predictions in unstructured populations, where this lag always stabilized eventually. As in the model of Marshall et al. (2016), Cotto and Ronce (2014) assumed, however, that different traits affected different stages in the life cycle.

Here we build on such previous theory (using in particular the methodological framework developed by Barfield et al. 2011 and Engen et al. 2011) to explore the evolution of lags in adaptation and extinction thresholds in changing environments in a stage-structured population with overlapping generations, considering that the same phenotypic traits affect different vital rates, in turn generating a trade-off. Our assumptions thus differ from previous models of adaptation to climate change but align with the empirical observations of opposite selection on the same trait reviewed above (e.g., Wadgymar et al. 2017). Engen et al. (2011) considered the evolution of such a phenotypic trait affecting age-specific survival rates and fecundities, with potentially different optimal values maximizing different vital rates, in a stationary stochastic environment with weak fluctuations (see also Childs et al. 2016). Under weak selection, Engen et al. (2011) found that evolution of the trait was well predicted when considering that it tracked an integrative optimal value, which is a weighted average of optima for each fitness component, where weights depend on elasticities. We here extend the weak selection results of Engen et al. (2011) to a stage-structured population facing directional change in its environment. Environ-

mental change is mimicked by assuming that the optimal phenotypic values for each vital rate change linearly through time, consistent with previous moving optimum theory. Our aim is to investigate how conflicting selection pressures and variable contributions to total fitness affect the evolution of the phenotype and adaptive lags between mean phenotype and stage-specific optima. In turn, we investigate the consequences of these adaptive lags for life histories in a changing environment. We ask whether feedbacks between evolution of phenotype and change in life history significantly alter adaptive trajectories in structured populations. We show that lag in adaptation in a structured population facing a changing environment may result in a shift along the trade-off between vital rates, with negative consequences for some fitness components but, less intuitively, improvements in some others. Complex eco-evolutionary dynamics can emerge in our model due to feedbacks between population demography and adaptation. Because of such feedback loops, selection may favor further shifts in life history in the same direction as those caused by maladaptive lags. These shifts in life history could be wrongly interpreted as adaptations to the new environment, while in reality they only reflect the inability of the population to adapt fast enough.

Methods

We first derive a general model for the joint evolution and demography of a stage-structured population facing a steadily changing environment, based on results of Barfield et al. (2011) and assuming Gaussian stabilizing selection on some (possibly multivariate) phenotype with an optimum moving in time, as in Orive et al. (2017). Our model allows for phenotypic plasticity, with a labile phenotype changing repeatedly as a function of the environment during the life of an individual. This assumption is motivated by the fact that many empirical examples of conflicting selection pressures across different fitness components concern phenological traits, which typically exhibit this form of plasticity. Exploring the evolution of reaction norms is, however, much beyond the aims of the present article, and we assume no genetic variation for the slope of the reaction norm. The model assumes that phenotypes and breeding values for the evolving phenotypic trait in each stage have a multivariate normal distribution with constant genetic and phenotypic variance-covariance matrices. We further assume weak selection such that the population reaches its stable stage structure quickly relative to its evolutionary dynamics. All stages then evolve at the same rate (Lande 1982; Barfield et al. 2011; Engen et al. 2011). These assumptions allow us to derive a general expression for the mean phenotype at equilibrium in a constant environment similar to Engen et al. (2011), as well as a general expression for the adaptive lag and genetic load affecting each life-history component in a changing environment.

We then illustrate the predictions of this general model using a simple life cycle with only two stages, distinguishing immature (nonreproductive) and mature (reproductive) individuals. We consider selection on a single phenotypic trait with divergent optima across two transitions in the life cycle, similar to the evolution of flowering time in the long-lived perennial plant *Boechera stricta* (Wadgymar et al. 2017). In the section "A Second Numerical Example: Evolution of Budburst Date in *Fagus* Species" in the appendix (available online), we show a second numerical example simulating the evolution of budburst date in a long-lived tree (Vitasse 2013).

General Model

Demography. We consider a population where the life cycle of individuals includes a number of discrete stages. Our demographic model assumes that the population is censused at regular intervals. We define a_{ij} as the total transition rate from stage j to stage i during such an interval. The population dynamics can then be described by the Lefkovitch matrix $\mathbf{A}_t = (\bar{a}_{ij})_t$, where $\bar{a}_{ij}$ is the mean transition rate given the distribution of phenotypes in stage j (see below) across one time step (for the sake of simplicity, the dependence on time has been omitted in the notation for these rates). Below we describe the (mean) transition rates $\bar{a}_{ij}$ alternatively as vital rates, life-history traits, or life-history components, to reflect a variety of terminologies that have been used in the literature. The change in the number of individuals in each stage is then governed by the equation $\mathbf{N}_{t+1} = \mathbf{A}_t\mathbf{N}_t$, where $\mathbf{N}_t$ is the population vector containing the total number of individuals in each stage at time t. We ignore the density dependence of vital rates (similar qualitative conclusions were, however, reached in a version of our model where the survival of the first stage in the life cycle was density dependent; results not shown). Our deterministic model also neglects demographic stochasticity and genetic drift, which amounts to considering large-enough populations.

Phenotypes. Within this life cycle, we assume that transitions between stages depend on some (possibly multivariate) expressed phenotype $\mathbf{x}$. For the same individual, this phenotype (e.g., breeding time) may vary plastically throughout life in response to some environmental cue ε_t (e.g., deviation in spring temperature with respect to some reference situation). We define as $\mathbf{z}$ the phenotype that the individual would express in the reference environment where $\varepsilon = 0$. We assume a linear reaction norm, such that the phenotype of an individual in stage i at time t is

$$\mathbf{x}_{i,t} = \mathbf{z} + \mathbf{b}_i\varepsilon_t = \mathbf{g} + \mathbf{e} + \mathbf{b}_i\varepsilon_t, \quad (1)$$

where $\mathbf{g}$ is the random vector containing the additive genetic value (breeding value) of each component of $\mathbf{x}$ in a reference environment where $\varepsilon = 0$ and $\mathbf{b}_i$ contains the slopes of the

plastic response of an individual in stage i to the environmental cue at time t for each component of $\mathbf{x}$. We here assume that plasticity may differ depending on the stage of the individual but that all individuals in the same stage have the same response to the environmental cue (no genetic variation on the slope of the reaction norm). This model also assumes that the phenotype of an individual at time t depends on its stage and current environmental cue but not on the past environments that the individual experienced in previous time steps, which are reasonable assumptions for many phenological traits. Finally, $\mathbf{e}$ is the random vector of residual values for a given individual (permanent environment effect). Following Barfield et al. (2011), we assume that the joint distribution of phenotypes and breeding values is Gaussian with mean $\bar{\mathbf{g}}_{i,t}$ and $\bar{\mathbf{z}}_{i,t}$ and variance-covariance matrices $\mathbf{P}_i$ and $\mathbf{G}_i$ (which can change with stage). In the following, we will track the evolution of the phenotype $\mathbf{z}$ (see also Childs et al. 2016) as if individuals were phenotyped in a common-garden experiment (e.g., Franks et al. 2014).

How Phenotypes Affect Demography. The probability of transition from stage j to stage i of an individual with expressed phenotype $\mathbf{x}$ at time t is given by

$$a_{ij} = A_{ij} \exp\left(-\frac{1}{2}(\mathbf{x} - \boldsymbol{\Theta}_{ij,t})^{\mathrm{T}} \mathbf{W}_{ij}^{-1} (\mathbf{x} - \boldsymbol{\Theta}_{ij,t})\right), \quad (2)$$

where $\boldsymbol{\Theta}_{ij,t}$ is the value of $\mathbf{x}$ that maximizes the transition from stage j to stage i at time t and A_{ij} is the maximal transition rate from stage j to stage i. The positive definite matrix $\mathbf{W}_{ij}$ determines how fast the transition rate a_{ij} between stages j and i declines when the expressed phenotype is displaced from $\boldsymbol{\Theta}_{ij,t}$ in different directions of the phenotypic space (lower values give a faster drop). We can express these transitions as functions of the phenotype $\mathbf{z}$ in the reference environment:

$$a_{ij} = A_{ij} \exp\left(-\frac{1}{2}(\mathbf{z} - \boldsymbol{\theta}_{ij,t})^{\mathrm{T}} \mathbf{W}_{ij}^{-1} (\mathbf{z} - \boldsymbol{\theta}_{ij,t})\right), \quad (3)$$

where $\boldsymbol{\theta}_{ij,t} = \boldsymbol{\Theta}_{ij,t} - \mathbf{b}_i \varepsilon_t$ is the optimum value of $\mathbf{z}$, which maximizes the transition from stage j to stage i at time t. Equation (3) allows different transitions in the life cycle to have different optimal phenotypes. This generates a tradeoff between these transitions, as phenotypic values maximizing one transition rate may displace another transition from its maximum rate.

Integrating over the (multivariate) Gaussian distribution of $\mathbf{z}$ at time t, the natural logarithm of the mean transition rate from stage j to stage i can be decomposed as

$$\begin{aligned} \ln(\bar{a}_{ij}) = {} & \ln(A_{ij}) + \frac{1}{2}\ln(|\mathbf{V}_{ij}^{-1}\mathbf{W}_{ij}|) \\ & - \frac{1}{2}(\bar{\mathbf{z}}_{j,t} - \boldsymbol{\theta}_{ij,t})^{\mathrm{T}} \mathbf{V}_{ij}^{-1} (\bar{\mathbf{z}}_{j,t} - \boldsymbol{\theta}_{ij,t}), \end{aligned} \quad (4)$$

where $\mathbf{V}_{ij}^{-1} = (\mathbf{W}_{ij} + \mathbf{P}_j)^{-1}$. This expression allows analysis of how different types of genetic loads constrain the demography of the population and its life cycle. The mean transition rate from stage j to stage i declines when the mean phenotype of stage j individuals departs from the specific optimal value maximizing this transition: the corresponding evolutionary or lag load (Lande and Shannon 1996) is measured by the third term on the right-hand side of equation (4). When the mean phenotype matches this optimal value, the mean transition rate from stage j to stage i declines when the phenotypic variance in stage j increases: the corresponding standing or variance load (Lande and Shannon 1996) is measured by the second term on the right-hand side of equation (4).

Environmental Change. The expressed phenotype maximizing each transition depends on some environmental value ε'_t (e.g., deviation in summer temperature), which may differ from the environmental cue affecting the plastic expression of the phenotype (see eq. [1]), with

$$\boldsymbol{\Theta}_{ij,t} = \boldsymbol{\Theta}_{ij,\varepsilon'=0} + \mathbf{B}_{ij}\varepsilon'_t,$$

where $\mathbf{B}_{ij}$ measures how the expressed phenotype maximizing transition between stage i and stage j changes with the environment (described as the "environmental sensitivity of selection" by Chevin et al. 2010). Note that selection on different stages may then vary with the environment in different manners, with some stages experiencing rapid changes in selection as the environment changes and some being unaffected (see also Marshall et al. 2016).

We here assume that both the environmental cue that affects phenotypic expression and the environmental value that affects selection on that phenotype change directionally through time at rate k; that is, $\varepsilon_{t+1} - \varepsilon_t = \Delta\varepsilon_t = \Delta\varepsilon'_t = k$ (as in Chevin et al. 2010). More general patterns of variation in the environment (e.g., with random fluctuations) are left for future work.

Focusing on the phenotype $\mathbf{z}$ in the reference environment, the rate of change in the optimal phenotype maximizing the transition rate between stage j and stage i is (see also Chevin et al. 2010)

$$\Delta\boldsymbol{\theta}_{ij,t} = k(\mathbf{B}_{ij} - \mathbf{b}_j) = k\boldsymbol{\beta}_{ij}, \quad (5)$$

with $\boldsymbol{\beta}_{ij} = \mathbf{B}_{ij} - \mathbf{b}_j$ being a measure of the sensitivity of that specific transition in the life cycle to environmental change, integrating the effect of stage-specific phenotypic plasticity. In other words, $\boldsymbol{\beta}$ measures how the mismatch between the expressed phenotype and the optimum changes with the environment.

Change in Phenotypes under Weak Selection

Assuming weak selection and that the population dynamics are faster than the evolutionary dynamics, the mean pheno-

typic value and the mean breeding value asymptotically evolve at the same rate in each stage (Lande 1982; Barfield et al. 2011), given by

$$\Delta\bar{\mathbf{z}} = \bar{\mathbf{z}}_{t+1} - \bar{\mathbf{z}}_t = \sum_{i,j} u_j v_i \frac{\bar{a}_{ij}}{\lambda} \mathbf{G}_j \nabla_{\bar{\mathbf{z}}_{j,t}} \ln \bar{a}_{ij} = \sum_{i,j} e_{ij} \mathbf{G}_j \nabla_{\bar{\mathbf{z}}_{j,t}} \ln \bar{a}_{ij}, \quad (6)$$

where $\nabla_x y = (\partial y/\partial x_1, \ldots, \partial y/\partial x_n)$ is the gradient operator and λ, the leading eigenvalue of $\mathbf{A}_t$, is the growth rate of the population once the stable stage structure has been reached. The right eigenvector $\mathbf{u}$ of $\mathbf{A}_t$ gives the stable stage structure—that is, the frequency of each stage at equilibrium—and its left eigenvector $\mathbf{v}$ gives the reproductive value of individuals in each stage, which measures their contribution to the growth rate of the population. Those vectors are normalized so that $\mathbf{u} \cdot \mathbf{v} = 1$. Equation (6) shows that evolution of the mean phenotype depends on selection gradients computed on each transition in the life cycle, weighted by the genetic variance in the concerned stage and demographic elasticities. The latter measure how proportional disturbances of transitions in the life cycle proportionally affect the population growth rate and are computed as $e_{ij} = \partial \ln \lambda / \partial \ln \bar{a}_{ij} = (\bar{a}_{ij}/\lambda) u_j v_i$ (Caswell 2001). Using equation (4) and further assuming that with weak selection the genetic variance and mean phenotype do not vary across stages (i.e., $\mathbf{G}_i = \mathbf{G}$ and $\bar{\mathbf{z}}_i = \bar{\mathbf{z}}$ for all stages i), the change in mean phenotype is

$$\Delta\bar{\mathbf{z}} = \mathbf{G} \sum_{i,j} e_{ij} \mathbf{V}_{ij}^{-1} (\boldsymbol{\theta}_{ij,t} - \bar{\mathbf{z}}_t) = \mathbf{G} \tilde{\mathbf{V}}^{-1} (\tilde{\boldsymbol{\theta}}_t - \bar{\mathbf{z}}_t), \quad (7)$$

where

$$\tilde{\mathbf{V}}^{-1} = \sum_{i,j} e_{ij} \mathbf{V}_{ij}^{-1} \quad (8)$$

is an integrative measure of the strength of stabilizing selection on the phenotype and

$$\tilde{\boldsymbol{\theta}}_t = \sum_{i,j} e_{ij} \tilde{\mathbf{V}} \mathbf{V}_{ij}^{-1} \boldsymbol{\theta}_{ij,t} \quad (9)$$

is an integrative measure of the optimal phenotype at time t. This optimal value integrates the effect of the trait throughout the life cycle, weighting its effect on each stage and life-history component by both the relative strength of selection within that life-history component (as measured by $\mathbf{V}_{ij}^{-1}$) and the contribution of that life-history component to total fitness (as measured by elasticities e_{ij}). Equations (7)–(9) are similar to expressions derived by Engen et al. (2011) for weak selection in an age-structured population.

Application: Evolution of Phenology in a Life Cycle with Two Stages

For the numerical exploration of our general model, we consider a simple life cycle with only two stages, which correspond to mature (reproductive) and immature (nonreproductive) individuals of a plant species (fig. 1). We census the population each year after flowering, when the reproductive status of individuals is known but seeds have not been released yet. A reproductive individual produces on average f_M seeds, of which a proportion s_0 will survive and develop into an immature individual the next year. Individuals never reproduce in their first year, and they may stay several years in the immature stage before they do. An immature individual survives to the next flowering season with probability s_I. Surviving immature individuals can then become reproductive with probability m or remain in the immature stage. Mature (reproductive) individuals survive from one year to another with probability s_M. We do not allow individuals already in the mature stage to skip reproduction for one or several years and return in the nonreproductive stage (no reversion or regression in the life cycle).

The study by Wadgymar et al. (2017) suggests that the optimal flowering time in *B. stricta* that maximizes fecundity of flowering individuals is earlier than the flowering time that would maximize their survival. Wadgymar et al. (2017) report selection patterns on other phenotypic traits than flowering time, but for simplicity of illustration we focus on this trait only. Note that constraining phenotypic variation to a single dimension increases the scope for antagonistic selection. We assume that flowering time does not affect the survival of nonreproductive individuals. Values of optimal flowering times for fecundity and survival as well as the strength of stabilizing selection, heritability, and phenotypic variance were inspired by estimates of fitness landscapes in Wadgymar et al. (2017). Estimates of speed of environmental change were taken from Anderson et al. (2012). To parameterize the average transition rates in the life cycle, we used a published life cycle for the related species *Boechera fecunda* (from the COMPADRE

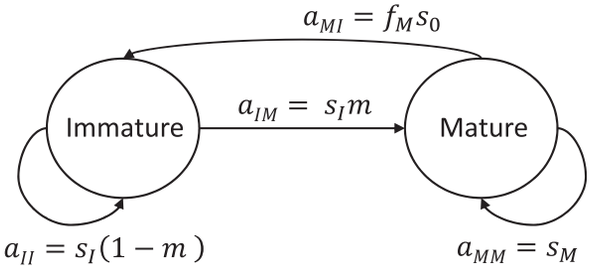

Figure 1: Life-cycle model. The subscripts I and M are used for immature (nonreproductive) and mature (reproductive) individuals, respectively. The census is after flowering and before seed release. Each transition from one stage to another between two censuses is represented by an arrow, with the corresponding transition rate computed by taking into account successive events leading to that transition between two censuses; for instance, an immature (nonreproductive) individual at time t is recorded as reproductive during census at time $t + 1$ if it survived as an immature (with probability s_I) and then flowered (with probability m).

database; Salguero-Gómez et al. 2015), another long-lived perennial plant. Such a life cycle provides values for transition rates $\bar{a}_{ij}$ in a reference environment ($\varepsilon = 0$) at equilibrium. We used these transition rates to compute values for demographic elasticities e_{ij} in that reference environment at equilibrium. From them, we computed the integrative optimal phenotypic value using equation (9). Replacing the value of the mean phenotype by this optimum equilibrium value in equation (4), we obtained estimates for the maximal transition rates A_{ij}, which were then used in further simulations assuming different environments. Parameter values for our reference scenario are shown in table 1. A second numerical example simulates the evolution of budburst date with effects on immature survival and adult fecundity in a long-lived tree species (shown in the section "A Second Numerical Example: Evolution of Budburst Date in *Fagus* Species" in the appendix).

In our numerical simulations, we iterated equation (7) to obtain trajectories for the mean phenotype. Transition rates were computed at each time point given the value of the mean phenotype, and elasticities were computed from the eigenvalues and eigenvectors of matrix $\mathbf{A}_t$. In fig. A1 (figs. A1–A7 are available online), we relax the assumption of weak selection and compare the dynamics of trait evolution to those predicted by equation (7). To examine the impact of feedbacks between demography and evolution on the dynamics of adaptation, we also contrasted the predictions of the model using equation (7) when elasticities change with maladaptation versus when constraining these elasticities to a constant reference value. The corresponding notebooks are deposited in the Dryad Digital Repository (https://doi.org/10.5061/dryad.2g7g3dc; Cotto et al. 2019).

Results

Constant Environment

Equation (7) predicts that in a constant environment, the mean phenotype evolves to an equilibrium value given by equation (9):

$$\lim_{t \to +\infty} \bar{\mathbf{z}}_t = \tilde{\boldsymbol{\theta}} = \sum_{i,j} e_{ij} \tilde{\mathbf{V}} \mathbf{V}_{ij}^{-1} \boldsymbol{\theta}_{ij}. \tag{10}$$

This evolved phenotype corresponds to an optimal compromise, which maximizes the growth rate of the population given the trade-offs between the different transitions in the life cycle. This optimal compromise depends on how different transitions contribute to total fitness as measured by demographic elasticities, which is a classic result of life-history theory (e.g., Hamilton 1966). This global optimum departs from the phenotype maximizing specific transitions in the life cycle. The phenotypic mismatches at equilibrium in a constant environment, measured by $\lim_{t \to +\infty} \bar{\mathbf{z}}_t - \boldsymbol{\theta}_{ij} = \tilde{\boldsymbol{\theta}} - \boldsymbol{\theta}_{ij}$ for each vital rate from stage i to stage j, generates variable evolutionary loads across different transitions in the life cycle (see eq. [4]), with consequences for life history.

Equation (10) predicts that the mean phenotype at equilibrium will lie closer to the optimal value for some specific transition if the evolving phenotype has a large effect on this transition and if the elasticity of the population growth rate with respect to disturbance in this transition is large. This is illustrated in figure 2: when the probability of becoming reproductive between two censuses is low, individuals spend on average several years in the immature stage before flowering and many will die before ever doing so. As a consequence, the elasticity of population growth rate to variation in fecun-

Table 1: Parameter notations and default values for our numerical example

Notation	Parameter	Default value for *Boechera* species
$\overline{f_M s_0}$	Number of new recruits per reproductive individual	3 (3.96)
$\bar{s}_I$	Annual survival rate of immature individuals	.7
m	Probability of becoming reproductive conditional on survival in the immature stage	.3
$\bar{s}_M$	Annual survival rate of mature individuals	.17 (.78)
W	Width of the selection function (for all transitions, in days^2)	40
P	Phenotypic variance (for both stages, in days^2)	24
$h^2 = G/P$	Heritability	.25
θ_{MI}	Optimal budburst (or flowering) date for fecundity (in Julian days) in the initial environment	152
β_{MI}	Sensitivity of θ_{MI} to the environmental change	−1
θ_{MM}	Optimal flowering time for reproductive individual survival (in Julian days)	167
β_{MM}	Sensitivity of θ_{MM} to the environment	−1
k	Speed of environmental change	.15

Note: For vital rates, the table shows the average value of that transition rate in a constant environment and, in parentheses, the maximal value of that transition rate.

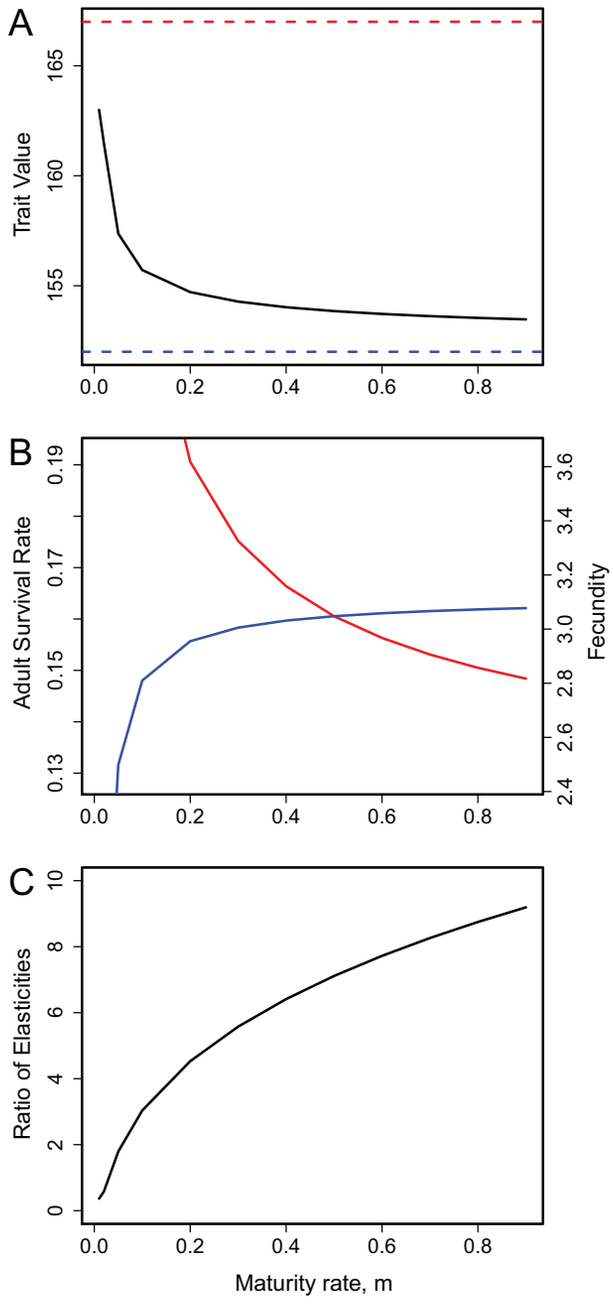

Figure 2: Equilibrium trait value (*A*), vital rates (*B*), and ratio of elasticities (*C*) as a function of the maturation rate. In *A*, the dashed blue line indicates the optimum for fecundity, the dashed red line indicates the optimum for adult survival, and the continuous black line indicates the trait value at equilibrium predicted using equation (10), all in Julian days. In *B*, the blue line indicates fecundity, and the red line indicates the survival rate of reproductive individuals. The scale of the *Y*-axes is ±20% of the vital rate values at $m = 0.5$. *C* shows the ratio of the elasticity to fecundity to the elasticity to adult survival, e_{MI}/e_{MM}. To obtain values for elasticities and vital rates at equilibrium, we iterated equation (7) for 5,000 time steps, starting with a mean phenotype equal to the optimal value maximizing adult survival, that is, $\bar{\mathbf{z}}_0 = \theta_{MM}$. For other parameter values, see table 1.

dity is small, and population growth depends mostly on the survival of mature individuals (fig. 2*C*). As a result, the optimal flowering time toward which the mean phenotype evolves lies closer to the value maximizing adult survival than to the optimum for fecundity (fig. 2*A*). When the maturation rate increases and the immature stage is shorter, the elasticity of population growth rate with respect to variation in fecundity increases (fig. 2*C*). The optimal flowering time that maximizes the population growth rate thus gets closer to the optimum for fecundity and further from the optimum for adult survival. Variation in the optimal flowering time in turn results in the evolution of different life histories as the maturation rate increases: evolution of earlier flowering is associated with increasing fecundity and decreasing adult survival (fig. 2*B*), and thus shorter life span.

The apparent simplicity of equation (10) hides the fact that elasticities depend on the evolution of the mean phenotype (such as flowering time), resulting in complex feedbacks between the demography of the population and its evolution. In figure 3, we explore these feedbacks by varying the distance between the optima maximizing different fitness components, thus changing the strength of the life-history trade-off. We contrast the predictions of equation (10) in two alternative scenarios: when elasticities are computed as a function of the evolving mean phenotype (thus allowing for eco-evolutionary feedbacks) versus when elasticities are assumed to stay constant at their value when the demographic transitions have the same optimum.

As the distance between optima starts to increase, the mean flowering time evolves to an intermediate value, well predicted when ignoring changes in elasticities (fig. 3*A*). But beyond a critical strength of the life-history trade-off (as measured by the distance between the optima for survival and fecundity), the equilibrium trait value diverges from the expectation under constant elasticities and gets closer to the fecundity optimum (fig. 3*A*). For even larger distances between optima, flowering time evolves to match the date maximizing fecundity only, at the expense of adult survival (fig. 3*A*). The population then becomes almost semelparous, with large fecundity and very low survival after flowering (fig. 3*B*). Interestingly, this radical shift in life history is not predicted when assuming constant elasticities (fig. 3*A*) and is thus driven by feedbacks between demography and evolution. This feedback occurs because as maladaptation in the mature stage becomes large, it depresses adult survival, which in turn lowers the contribution of adult survival to the population growth compared with fecundity (fig. 3*C*), thus weakening selection on adult survival. Weaker selection results in the evolution of even greater genetic load and maladaptation for this specific fitness component, while adaptation is improved for the other fitness component (fecundity), as it becomes released from the life-history trade-off. This positive feedback loop thus results in a shift in the life cycle, with a collapse of adult survival

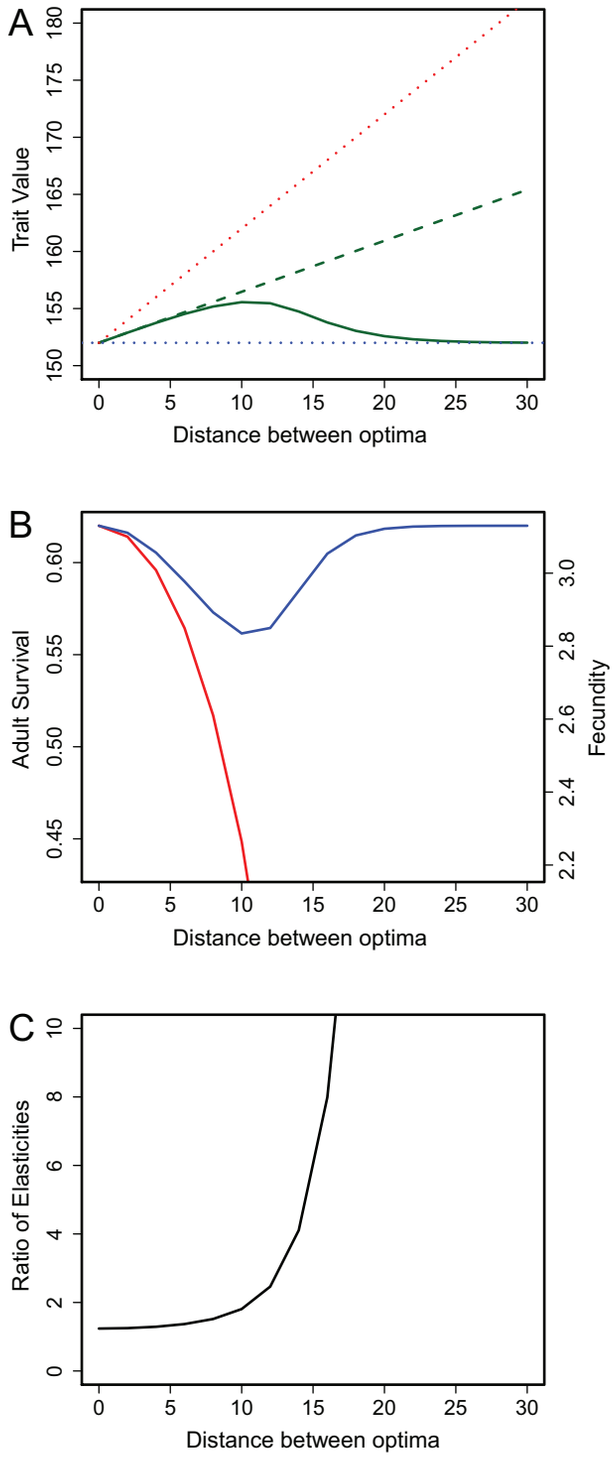

Figure 3: Trait values at equilibrium, vital rates, and ratio of elasticities as a function of the intensity of the potential life-history trade-off, quantified by the distance between the optima. In *A*, the dotted blue line indicates the optimum for fecundity ($\theta_{MI} = 152$), the dotted red line indicates the optimum for adult survival ($\theta_{MM} = \theta_{MI} + \delta$, where δ represents the distance between the optima [*X*-axis]), the continuous green line indicates the equilibrium trait value predicted using equation (10), and the dashed green line indicates the equilibrium trait value predicted using equation (10) with constant elasticities equal to their value when the optima are identical. All phenotypic values are in Julian days. In *B*, the blue line indicates mean fecundity, and the red line indicates adult survival rate. The scale of the *Y*-axes is within −30% of the vital rate values when the optima are equal. *C* shows the ratio of the elasticity to fecundity to the elasticity to adult survival, e_{MI}/e_{MM}. To obtain values for mean phenotype, elasticities, and vital rates at equilibrium, we iterated equation (A2) for 3,000 time steps, starting with all phenotypic and breeding values equal to the optimal value maximizing adult fecundity, that is, $\bar{\mathbf{z}}_0 = \theta_{MI}$. For other parameter values, see table 1.

and specialization on fecundity, mediated by the evolution of flowering time.

When the distance between optima is large, we also observed multiple alternative equilibria in this scenario: populations with a mean phenotype initially close to the optimum for adult survival failed to evolve toward semelparity and eventually became extinct (results not shown), while populations with an initial mean phenotype close to the optimum for fecundity evolved toward semelparity and persisted (fig. 3). These multiple alternative equilibria are associated with multiple peaks in the fitness landscape relating population growth rate to flowering time (fig. A2). Populations with a mean phenotype close to the optimum maximizing survival are trapped on a local fitness peak, which does not allow persistence.

Changing Environment: Lag in Overall Adaptation

In a changing environment, we expect the mean trait value to lag behind the optimal phenotype due to evolutionary inertia (Lande and Shannon 1996). To make analytical progress, we here assume that under weak selection in a changing environment, the population reaches an asymptotic dynamic state where its demographic properties are approximately constant but different from those in a stable environment. Under such a conjecture, if the mean phenotype tracks its global optimum with a constant lag, substituting equation (5) in equation (9) and solving for a constant lag leads to

$$\lim_{t \to +\infty} (\tilde{\boldsymbol{\theta}}_t - \bar{\mathbf{z}}_t) = k\tilde{\mathbf{V}}\mathbf{G}^{-1}\tilde{\boldsymbol{\beta}}, \tag{11}$$

where $\tilde{\boldsymbol{\beta}} = \sum_{ij} e_{ij}\tilde{\mathbf{V}}\mathbf{V}_{ij}^{-1}\boldsymbol{\beta}_{ij}$ is an integrative measure of the sensitivity of the population growth rate to environmental change, mediated by several components of fitness. This expression for the phenotypic lag in the asymptotic regime is similar to that predicted by Lynch et al. (1991) and Lande and Shannon (1996) in the univariate case and by Gomulkiewicz and Houle (2009) and Chevin (2013) in the multivariate case. Equation (11) suggests that the lag increases when the environment changes fast, when selection is weak, and when there is little genetic variance in the direction of environmental change, as found by previous studies in unstructured populations. In the case of a stage-structured population, equa-

tion (11) and the definition of $\tilde{\boldsymbol{\beta}}$ additionally suggest that the overall phenotypic lag will be larger if those transitions with the largest contribution to the population growth rate (as measured by elasticities e_{ij}) are very sensitive to environmental change in phenotypic directions where plasticity does not allow tracking the optimum (as measured by $\boldsymbol{\beta}_{ij}$).

Changing Environment: Consequences for Life-History Components

We here analyze how the mean phenotype in a changing environment departs from the optimum maximizing each transition using the prediction for the lag in the asymptotic regime in equation (11). This phenotypic mismatch is directly related to the evolutionary load depressing the different components of the life cycle, as shown in equation (4). The mismatch specific to each transition thus allows exploring how the changing environment may affect the life history of individuals. If the mean phenotype tracks the global optimum with a constant lag, we have

$$\boldsymbol{\theta}_{ij,t} - \bar{\mathbf{z}}_t = (\boldsymbol{\theta}_{ij,t} - \tilde{\boldsymbol{\theta}}_t) + k\tilde{\mathbf{V}}\mathbf{G}^{-1}\tilde{\boldsymbol{\beta}}. \quad (12)$$

Equation (12) predicts that the phenotypic mismatch affecting a specific transition in the life cycle depends (i) on how the global optimal phenotype departs from the phenotypic value maximizing that transition rate (first term on the right-hand side of eq. [12]), as in a constant environment, illustrated in figures 2 and 3; and (ii) on the lag between the mean phenotype and global optimal phenotype (second term on the right-hand side of eq. [12]).

If we ignore the feedbacks between evolution and demography and assume that the elasticities stay approximately constant in a changing environment and equal to their initial values in a stable environment, then the global optimal phenotype changes approximately linearly in time, $\tilde{\boldsymbol{\theta}}_t = \tilde{\boldsymbol{\theta}}_0 + k\tilde{\boldsymbol{\beta}}t$, and we can further express the phenotypic mismatch affecting the transition between stages j and i as

$$\boldsymbol{\theta}_{ij,t} - \bar{\mathbf{z}}_t = (\boldsymbol{\theta}_{ij,0} - \tilde{\boldsymbol{\theta}}_0) + kt(\boldsymbol{\beta}_{ij} - \tilde{\boldsymbol{\beta}}) + k\tilde{\mathbf{V}}\mathbf{G}^{-1}\tilde{\boldsymbol{\beta}}. \quad (13)$$

Equation (13) shows that the phenotypic mismatch for a particular transition results from (i) the initial difference between the optimum for this transition and the global optimum, (ii) the difference between the effective sensitivity to environmental change of this transition (accounting for plasticity) and that of the global optimum, and (iii) the lag in overall adaptation, reflecting the inability to perfectly track the global optimum in time.

We first focus on the simple case where each transition in the life cycle has the same effective sensitivity to environmental change, that is, when $\boldsymbol{\beta}_{ij} = \tilde{\boldsymbol{\beta}} = \boldsymbol{\beta}$ for all i and j. In that case, the second term on the right-hand side of equation (13) vanishes. Equation (13) then predicts that the phenotypic mismatch (and thus evolutionary load) affecting the transition will also stabilize through time in the asymptotic regime. This evolutionary load will then be higher for some fitness components in a changing environment than in a stable environment, for example, when the lag in adaptation pushes the mean phenotype even further from the optimal value for that fitness component. For other fitness components, equation (13) predicts that the evolutionary load may be smaller in a changing environment than in a stable environment. This happens when the lag is not too large and pushes the mean phenotype away from the global optimum but closer to the optimal phenotype for that fitness component. Formally this happens when $\cos(\alpha) > (\|k\tilde{\mathbf{V}}\mathbf{G}^{-1}\tilde{\boldsymbol{\beta}}\|)/(2\|\boldsymbol{\theta}_{ij,0} - \tilde{\boldsymbol{\theta}}_0\|)$, where α is the angle between the initial mismatch for transition a_{ij} and the phenotypic lag, that is, between the first and last term on the right-hand side of equation (13). This is illustrated in figure 4 for our univariate example. The mean phenotype eventually tracks the global optimum with a constant lag, which is such that the mean flowering date is closer to the optimal date for adult survival in a changing environment than it is in a stable environment (fig. 4*A*). As a consequence, the mean fecundity decreases while the mean adult survival increases (fig. 4*B*). These shifts in life history could wrongly be interpreted as adaptations to the changing environment while they actually have a maladaptive origin: they are the consequences of the phenotypic lag that develops because the population is unable to track its moving optimum sufficiently fast.

The global optimum phenotype and equilibrium value of the phenotypic lag depart from those predicted assuming constant elasticities (fig. 4*B*). In particular, the lower evolutionary load on adult survival in a changing environment, relative to that in a constant environment, increases the elasticity of the population growth rate to adult survival compared with fecundity (fig. 4*C*). The contribution of the former to population growth increases and shifts the optimal compromise for flowering time toward the date maximizing adult survival. Interestingly, the eco-evolutionary feedbacks between demography and evolution then cause selection to favor further shifts in life history, in the same direction as those caused by maladaptive lags.

Predictions of lags in adaptation and phenotypic mismatches based on constant elasticities perform less well when the environment changes faster (fig. 5*A*). Ignoring feedbacks between demography and evolution also leads to overestimations of the critical rate of environmental change above which extinction is certain (fig. 5*B*). Interestingly, in our model the lag between the mean phenotype and the integrative optimum is not sufficient to predict survival or demise of the population: information about specific evolutionary loads affecting each life-history component is necessary.

We now turn to the case where different transitions in the life cycle have different effective sensitivities to environmen-

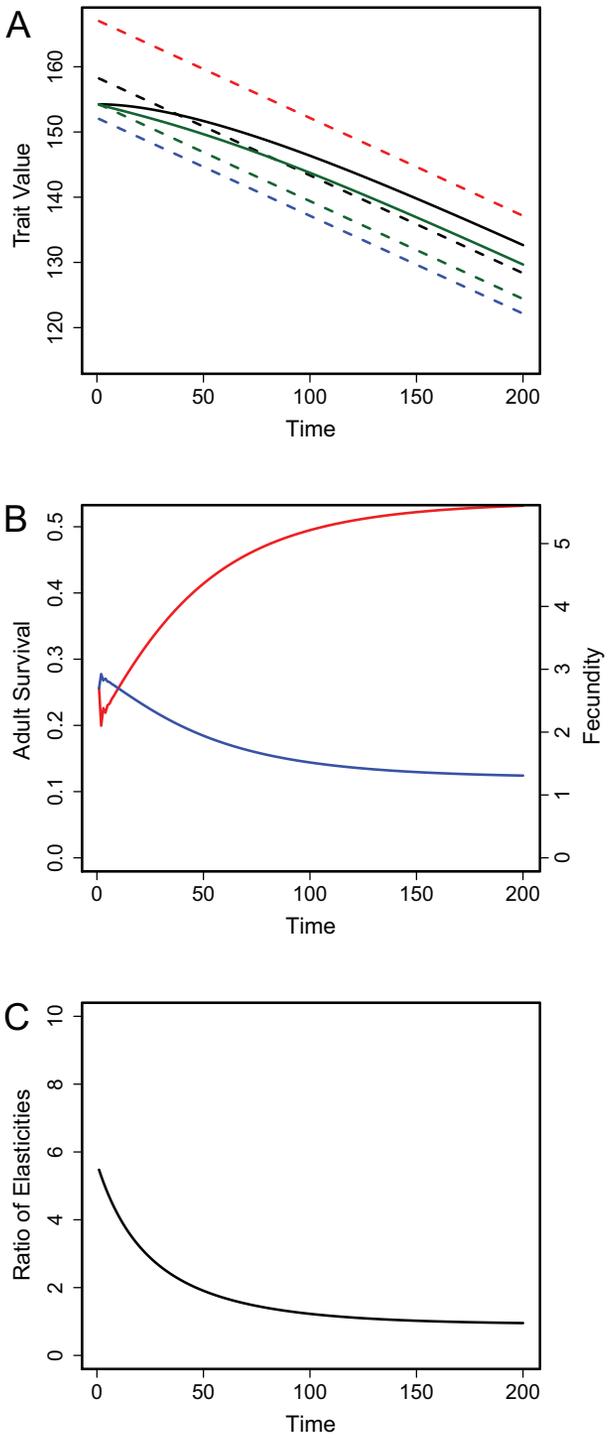

Figure 4: Change in trait value, vital rates, and ratio of elasticities as a function of time when the environment changes slowly (i.e., the population growth rate is greater than 1 at the equilibrium lag). In *A*, the dashed blue line indicates the optimum for fecundity, the dashed red line indicates the optimum for adult survival, the continuous green line indicates the global optimum predicted using equation (9) and recalculating elasticities at each time step, the dashed green line indicates the optimum predicted using equation (9) with constant elasticities as at time 0, the continuous black line indicates the mean adult phenotype predicted using equation (7), and the dashed black line indicates the trait value expected at the dynamic equilibrium using equation (13) with constant elasticities as at time 0. In *B*, the blue line indicates fecundity, and the red line indicates adult survival rate. The scale for the *Y*-axes is within 100% of the vital rate values at time 0. *C* shows the ratio of the elasticity to fecundity to the elasticity to adult survival, e_{MI}/e_{MM}. Vital rates and elasticities are computed at each time step using equation (A2). At time 0, the population is initialized with the mean phenotype and stage structure expected at equilibrium in our reference environment. Parameter values are as in table 1.

tal change (different $\boldsymbol{\beta}_{ij}$). If the sensitivity of the transition a_{ij} to the environment differs from the integrated sensitivity $\tilde{\boldsymbol{\beta}}$, equation (13) suggests that the phenotypic mismatch affecting this transition increases linearly with time. The induced maladaptation should lead the transition rate $\bar{a}_{ij}$ to vanish eventually (with speed also depending on $\mathbf{V}_{ij}$; eqq. [3], [4]), which in the case where it is the only transition to stage *i* leads to the disappearance of this stage. This may result in the extinction of the whole population or the evolution of a simpler life cycle, as in the life-cycle meltdown described in figure 3. In both cases, the demographic properties of the population are expected to change with increasing maladaptation, and our approximation based on constant elasticities is expected to eventually break down with time.

Our numerical simulations show that flowering time initially lags behind its optimum, as in figure 4*A*, and equation (13) predicts reasonably well the position of the mean phenotype (dashed black line in fig. 6*A*). In that period, fecundity decreases and adult survival increases (fig. 6*B*), as it did in figure 4*B*. Yet as the two optima diverge further, the distance between the optimal flowering time and the date maximizing survival increases, aggravating the evolutionary load depressing that vital rate. This change in demography reverses the direction of selection: the global optimal phenotype, which had begun to shift toward the survival optimum, now shifts back in the other direction to get closer to the fecundity optimum (figs. 6*A*, A4). Eventually, the global optimal phenotype converges with the fecundity optimum (continuous green line fuses with dashed blue line in fig. 6*A*), and the mean phenotype tracks the latter with some lag (black vs. green continuous line in fig. 6*A*), leading to the same type of evolution toward semelparity as in figure 3, with increasing fecundity and decreasing survival (fig. 6*B*). This transition from iteroparity to semelparity is associated with a strong transient reduction in population growth rate, as the optima for fecundity and survival diverge (fig. A3).

Figure 6*C* and 6*D* shows another interesting scenario that may be described as evolutionary trap, where the feedbacks between demography and evolution cause the optimal integrative optimum to shift toward the survival optimum and away from the semelparous strategy due to increasing lag in adaptation in a changing environment, as described in fig-

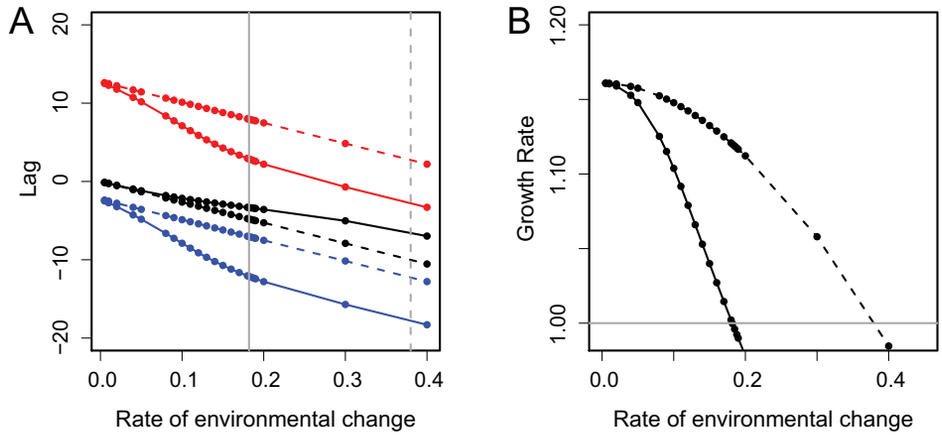

Figure 5: Lag in adaptation (*A*) and asymptotic growth rate (*B*) as a function of the rate of environmental change, *k*. In *A*, the continuous lines show the mismatches at dynamic equilibrium between mean trait value (from eq. [7]) and the optimum for survival (red), the optimum for fecundity (blue), and the global optimum (black, from eq. [9]). The dashed lines show the corresponding equilibrium lags but assuming constant elasticities set to their values when the environment is stable. The differences between continuous and dashed lines of the same color therefore reflect the influence of feedbacks between demography and evolution. The vertical continuous gray line represents the rate of change above which the population size actually decreases (corresponding to $\lambda < 1$ in *B*), whereas the vertical dashed gray line corresponds to the rate of change at which the population is predicted to decrease when assuming constant elasticities. In *B*, the continuous line shows the population growth rate when the mean phenotype is predicted with equation (7) after 10,000 time steps, and the dashed line shows the population growth rate when the mean phenotype is predicted from the equilibrium lag using equation (11) and the optimal phenotype is predicted using equation (9) with constant elasticities as when the environment is stable. The horizontal gray line is the boundary between a growing and a decreasing population size. At time 0, the population is initialized with the mean phenotype and stage structure expected at equilibrium in our reference environment. Equation (7) was iterated for 10,000 time steps to reach a dynamical equilibrium. Other parameter values are as in table 1.

ure 4. However, this local optimum in fitness is not viable, and the demise of the population is accelerated by those feedbacks. Contrary to the previous example, the population is trapped on this local optimum and unable to evolve toward the semelparous strategy, which would be viable in this changing environment. Interestingly, some vital rates (such as survival here in fig. 6*D*) keep increasing, but the population is nevertheless declining to extinction.

Discussion

Several recent empirical studies (Ehrlén and Münzbergová 2009; Mojica and Kelly 2010; Tarwater and Beissinger 2013; Vitasse 2013; Childs et al. 2016; Wadgymar et al. 2017) have suggested that conflicting selection pressures on the same phenotypic traits across different fitness components could play a key role in climatic adaptation, which has been little explored by previous theory. Inspired by these empirical examples, we have here theoretically explored the consequences of such conflicting selection on the adaptation and demography of a stage-structured population confronted with a changing environment, such as rising temperature under climate change. We have asked three questions: (i) How do conflicting selection pressures across different fitness components affect adaptation lags in a changing environment? (ii) How do such lags in adaptation in turn affect the vital rates, and thus the life cycle itself, in a changing environment? (iii) Can feedback loops between phenotypic evolution and life-history changes alter adaptive and demographic trajectories of structured populations facing climate change? We here discuss in turn the answers provided by our study to each of these questions and their relationships with other theoretical and empirical work.

Adaptation Lags in Stage-Structured Populations

The dynamics of adaptation in a stage-structured population are in general highly nontrivial. Assuming weak selection allowing the population to reach its stable stage structure fast (following Engen et al. 2011), we can, however, express the change in mean phenotype through time in very simple form, similar to that in an unstructured population. Responses to selection then depend on integrative measures of the optimal phenotype, strength of stabilizing selection around that optimum, and speed of environmental change. For each of these measures, the integration is made by weighting each characteristic (optimal phenotype, selection strength, and environmental sensitivity) specific to a transition in the life cycle by weights that depend on the corresponding demographic elasticity (Caswell 2001). Transitions in the life cycle that have a large contribution to the population growth rate are associated with large elasticities and thus have larger effects on lags in adaptation. The present theoretical results thus offer a simple mean to pre-

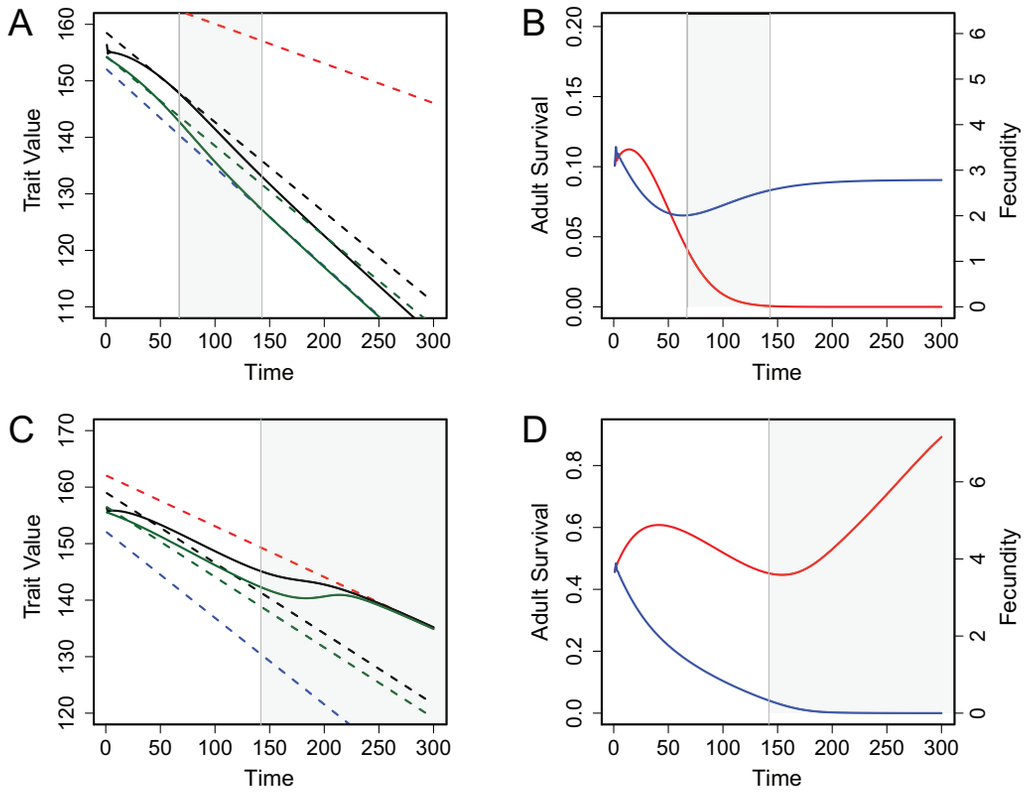

Figure 6: Trait value (*A*, *C*) and vital rates (*B*, *D*) as functions of time when the optima move with different speeds. In *A* and *C*, the dashed blue line indicates the optimum for fecundity, the dashed red line indicates the optimum for adult survival, the continuous green line indicates the global optimum predicted using equation (9) and recalculating elasticities at each time step, the dashed green line indicates the optimum predicted using equation (9) with constant elasticities as at time 0, the continuous black line indicates the mean phenotype predicted using equation (7), and the dashed black line indicates the trait value expected at the dynamic equilibrium using equation (11) with constant elasticities as at time 0. In *B* and *D*, the red line indicates adult survival, and the blue line indicates fecundity. The scale on the *Y*-axes is ±100% of the vital rate values in a constant environment. Vital rates and elasticities are computed at each time step using equation (2). In *A* and *B*, parameters are as in table 1, and $\beta_{IM} = -2.5$, $\beta_{MM} = -1$, and $k = 0.07$. For *C* and *D* we used other parameter values that fall into the possible range for estimated parameters in the *Boechera stricta* example, namely (using the same notations as in table 1), $\bar{fs}_0 = 3.51$ (4.63), $\bar{s}_M = 0.49$ (0.99), and $\theta_{MM} = 162$, with other parameters as in table 1 and $\beta_{IM} = -1.7$, $\beta_{MM} = -1$, and $k = 0.09$. At time 0, the population is initialized with the mean phenotype and stage structure expected at equilibrium in our reference environment. Gray areas represent situations where the population declines ($\lambda < 1$).

dict lags in adaptation in a large diversity of organisms from basic demographic information about their life cycles.

Given conflicts in selection across different vital rates, the integrative optimal phenotype that maximizes the population growth rate thus departs from the phenotype that is optimal for specific life-cycle transitions. Overall maladaptation can thus be severely overestimated or underestimated when focusing on a single fitness component. The few empirical studies that have estimated maladaptation through different fitness components concur with this conclusion. For instance, in populations of *Boechera stricta* the mean phenotype lies much closer, for several traits, to the optimum for survival than to the optimum for fecundity, with the phenotype maximizing lifetime fitness lying in between those two values (Wadgymar et al. 2017). Similarly, Ehrlén and Münzbergová (2009) found only weak selection on flowering time in *Lathyrus vernus* when integrating the conflicting selection pressures on this trait across the whole life cycle, despite consistent and strong directional selection on that trait when examining fecundity only.

Our model predicts that lag in adaptation will be smaller if life-cycle transitions with low demographic elasticity are the most sensitive to climate change. A classic prediction from life-history theory, largely confirmed by data, is that vital rates with a small contribution to population growth rate should be more variable and sensitive to environmental conditions, while vital rates with high elasticity should be more buffered (e.g., Morris and Doak 2004). Meta-analyses in marine environments suggest that larval pelagic stages are more sensitive to climate change than benthic adult stages (Przeslawski et al. 2015; see also the discussion in Marshall et al. 2016). In many long-lived organisms, the contribution of fecundity and im-

mature survival to population growth is minor in comparison to the contribution of adult survival. Our model thus suggests that we should be concerned when climate change becomes so intense that it affects adult mortality in long-lived species, as observed in some forest trees (e.g., van Mantgem and Stephenson 2007). This is of concern not only because of the direct demographic impact of climate change but also because of the increasing difficulty of tracking an environment that is perceived as changing faster through its integrative effects on the life cycle.

Marshall et al. (2016) also predicted larger lags in adaptation and higher extinction risk in a stage-structured population when some stages are more sensitive to climate change than others. Because of their assumption of nonoverlapping generations, Marshall et al. (2016)'s predictions are not framed as functions of demographic elasticities. They instead invoked general arguments about complexity limiting adaptation (much like other multivariate models of adaptation without explicit life cycles; e.g., Gomulkiewicz and Houle 2009; Duputié et al. 2012; Chevin 2013) to explain the increased susceptibility to extinction in life cycles with stages having a different ecology.

Shifts in Life History in a Changing Environment

As the integrative optimal phenotype changes through time, the mean phenotype will lag behind the value that maximizes the population growth rate. This lag results in a shift in life history compared with the optimal compromise because the distance between the mean phenotype and optima-maximizing specific vital rates is then modified differently for different vital rates. Moderate lag in adaptation causes increased evolutionary load for some fitness components but may also—and less intuitively—decrease evolutionary load for other fitness components. Consequently, some vital rates decline while some others improve when the environment changes. This pattern is reminiscent of patterns of demographic compensation, such as negative correlation between vital rates along environmental gradients described by Villellas et al. (2015) in a number of plant demographic data sets. In particular, Doak and Morris (2010) found in two tundra species that warmer temperature at the southern edge of their range was associated with lower survival and recruitment but higher growth of plants. Doak and Morris (2010) suggested that these opposite changes in life history could buffer for a while the negative effects of climate change. Different mechanisms, such as release from density dependence, may explain these patterns (Reed et al. 2013). Our model suggests a new mechanism through which such opposite changes in vital rates could emerge. These shifts in life history in our model are, however, maladaptive in that they result from the mean phenotype lagging behind the strategy with maximal growth in the current environment and are thus associated with a reduction in total fitness. Our model thus calls for caution when interpreting improvement of some fitness components as a sign of ongoing adaptation to climate change or beneficial effects of a warmer climate. In our simulations, improvement of some vital rates could instead signal increasing maladaptation and imminent extinction because they are associated with a strong decline in other fitness components.

Several empirical examples of conflicting selection on phenology suggest that the optimal phenology for fecundity is earlier than the optimum for survival (Ehrlén and Münzbergová 2009; Tarwater and Beissinger 2013; Wadgymar et al. 2017; but for the opposite pattern, see Childs et al. 2016). There is also substantial evidence that climate change favors the evolution of more precocious phenology (e.g., Anderson et al. 2012; see other examples in Franks et al. 2014). Under such a scenario, assuming that the optima for fecundity and survival are similarly advanced by climate change, our model predicts that the lag in adaptation, by causing the mean phenotype to be late relative to the integrative optimum, will make the former closer to the survival optimum than in a constant environment (as in the *Boechera* example in our simulations), increasing survival but decreasing fecundity. Climate change could thus explain why the mean phenotype seems to lie closer to the survival optimum in many empirical examples (Siepielski et al. 2011).

Feedback Loops between Demography and Evolution

We also asked whether changes in life history caused by lag load in a changing environment are of sufficient magnitude to feed back on selection on the mean phenotype and alter its evolutionary trajectory. To test this idea, we have systematically compared the evolution of the mean phenotype to predictions assuming no change in demographic elasticities, in effect neglecting effects of changes in life history on selection. Ignoring these feedbacks works well and produces reasonably accurate predictions when selection is weak, environmental change is slow, and changes in life history are constrained by hypotheses about the life cycle (see, e.g., the example of evolution of budburst date in a long-lived tree in the section "A Second Numerical Example: Evolution of Budburst Date in *Fagus* Species" in the appendix). However, even in this most favorable scenario predictions ignoring eco-evolutionary feedbacks perform less well close to extinction thresholds (fig. A7), where changes in life-history traits presumably grow in magnitude. In particular, ignoring feedbacks leads to overestimating the rate of change that the population can endure (figs. 5, A7), a conclusion reached by previous studies of adaptation in a changing environment for different types of feedbacks involving drift (Bürger and Lynch 1995) or strength of selection (Osmond and Klausmeier 2017).

Under stronger selection and/or faster environmental change our simulations showed complex evolutionary trajectories, driven in a large part by such feedback loops between demog-

raphy and evolution. Positive feedback loops emerge in our model because (i) a large phenotypic mismatch affects a life-history component (or vital rate) by increasing the genetic load depressing this vital rate; (ii) change in a vital rate diminishes the contribution of this transition to the population growth (as measured by its elasticity) and thus the strength of selection on that transition; (iii) as a result of this weaker selection, the integrative optimal phenotype is displaced farther away from the optimum for that transition; and (iv) the mean phenotype evolves to track the new global optimum, further increasing the phenotypic mismatch and the genetic load depressing this vital rate. Tarwater and Beissinger (2013) discussed similar positive feedback loops affecting the evolution of phenology in the parrotlet *Forpus passerines*, where lower rainfall would decrease selection on fecundity and increase selection on survival, pushing the optimal breeding date toward later dates, which in turn would further decrease fecundity. An interesting consequence of these feedback loops is that selection favors further shift in life history (through change in the integrative optimal phenotype) in the same direction as the maladaptive lags in a continuously changing environment. These changes in optimal phenotype are actually not directly due to the changing environment but to the lags in adaptation that develop in such environment and modify the life history.

Osmond and Klausmeier (2017) recently showed that relaxing the common assumption that selection strength always increases with the distance of the mean phenotype to the optimum leads to interesting dynamical behaviors typical of nonlinear systems. These include tipping points, with abrupt catastrophic transitions from positive to negative growth rates, and hysteresis, where the effects of environmental change cannot be reversed even after it has stopped (Osmond and Klausmeier 2017). The lag in adaptation may in particular never reach a steady state in their model. In the present model, the strength of selection on life-history components also does not always increase with increasing distance to the optimum, due to the demographic feedbacks described above. Lags in adaptation that increase without reaching a steady state were also found by Cotto and Ronce (2014) when investigating the evolution of traits affecting only older age classes in a changing environment, due to similar feedbacks involving changes in elasticities (see also E. Bouin, T. Bourgeron, V. Calvez, O. Cotto, J. Garnier, T. Lepoutre, and O. Ronce, unpublished results). These studies, as well as the present one, thus suggest that the complex dynamics described by Osmond and Klausmeier (2017) for some specific fitness functions could be quite general features of adaptation to a changing environment in stage-structured populations.

A specific property of stage-structured populations is, however, that these catastrophic transitions can affect only some transitions in the life cycle, thereby causing changes in the life cycle while still allowing persistence of the population. We here predicted cases of transitions toward semelparity, where the ability to survive after reproduction was lost due to increasing maladaptation affecting that life-history component. This disappearance of some stage or age classes in the life cycle, mediated by positive feedback loops and spirals of increasing maladaptation, could be described as a life-cycle meltdown, by analogy with previous theoretical predictions of meltdown due to mutation or migration loads (Lynch and Gabriel 1990; Ronce and Kirkpatrick 2001). Life-cycle meltdown leading to the evolution of semelparity was predicted in particular by models of mutation accumulation in age-structured populations (Wachter et al. 2013). By considering antagonistic selection across life-history components, our model also shares some conceptual features with models of niche evolution, which consider antagonistic selection across different environments (e.g., Ronce and Kirkpatrick 2001). In both cases, positive demographic feedbacks mediated by changes in elasticities play a major role in constraining adaptation and explaining the evolution of specialized life histories or ecological niches (Holt 1996).

Conclusion

Data suggest that traits involved in climatic adaptation are often under conflicting selection pressures across different fitness components. The present model shows that under climate warming, such antagonistic selection can result in shifts in life history that could be wrongly interpreted as adaptation to the new climate, while they only reflect the inability of the population to adapt fast enough. Interestingly, these maladaptive changes in life history in turn alter selection on phenotypes, leading to either evolutionary traps or evolutionary rescue through major changes in the life cycle. These feedbacks between adaptation, demography, and life history deserve further exploration under more complex patterns of environmental change, including random climatic fluctuations.

Acknowledgments

We acknowledge support from the European Research Council (grant FluctEvol ERC-2015-STG-678140 to L.-M.C.), from the Agence Nationale de la Recherche (project MeCC ANR-13-ADAP-0006), and from the Peter Wall Institute of Advanced Studies to O.R. We thank Sébastien Lavergne for pointing out interesting literature; Jill Anderson for helpful explanations about her and her colleagues' data set; Julie Gaüzere, Isabelle Chuine, and Bertrand Teuf for access to their unpublished results; and Andrew Hendry for comments on an early version of the article. The *Fagus* species scenario benefitted from discussions with all members of the MeCC project. Matthias Grenié did a short internship project under the supervision of L.-M.C. and O.R.; his simulations results, obtained using a similar model, are not included in the present article, but our understanding of the model did move for-

ward during that time. This is publication ISEM 2018-206 from the Institut des Sciences de l'Evolution, Montpellier.

Literature Cited

Aguilée, R., G. Raoul, F. Rousset, and O. Ronce. 2016. Pollen dispersal slows geographical range shift and accelerates ecological niche shift under climate change. Proceedings of the National Academy of Sciences of the USA 113:E5741–E5748.

Anderson, J. T., D. W. Inouye, A. M. McKinney, R. I. Colautti, and T. Mitchell-Olds. 2012. Phenotypic plasticity and adaptive evolution contribute to advancing flowering phenology in response to climate change. Proceedings of the Royal Society B 279:3843–3852.

Barfield, M., R. D. Holt, and R. Gomulkiewicz. 2011. Evolution in stage-structured populations. American Naturalist 177:397–409.

———. 2014. Correction. American Naturalist 184:284–287.

Bürger, R., and M. Lynch. 1995. Evolution and extinction in a changing environment: a quantitative-genetic analysis. Evolution 49:151–163.

Caswell, H. 2001. Matrix population models. Sinauer, Sunderland, MA.

Chevin, L.-M. 2013. Genetic constraints on adaptation to a changing environment. Evolution 67:708–721.

Chevin, L.-M., R. Lande, and G. M. Mace. 2010. Adaptation, plasticity, and extinction in a changing environment: towards a predictive theory. PLoS Biology 8:e1000357.

Childs, D. Z., B. C. Sheldon, and M. Rees. 2016. The evolution of labile traits in sex- and age-structured populations. Journal of Animal Ecology 85:329–342.

Cotto, O., and O. Ronce. 2014. Maladaptation as a source of senescence in habitats variable in space and time. Evolution 68:2481–2493.

Cotto, O., L. Sandell, L.-M. Chevin, and O. Ronce. 2019. Data from: Maladaptive shifts in life history in a changing environment. American Naturalist, Dryad Digital Repository, https://doi.org/10.5061/dryad.2g7g3dc.

Cotto, O., J. Wessely, D. Georges, G. Klonner, M. Schmid, S. Dullinger, W. Thuiller, and F. Guillaume. 2017. A dynamic eco-evolutionary model predicts slow response of alpine plants to climate warming. Nature Communications 8:15399.

Coulson, T., B. E. Kendall, J. Barthold, F. Plard, S. Schindler, A. Ozgul, and J.-M. Gaillard. 2017. Modeling adaptive and nonadaptive responses of populations to environmental change. American Naturalist 190:313–336.

Crozier, L. G., A. Hendry, P. W. Lawson, T. Quinn, N. Mantua, J. Battin, R. Shaw, and R. Huey. 2008. Potential responses to climate change in organisms with complex life histories: evolution and plasticity in Pacific salmon. Evolutionary Applications 1:252–270.

Doak, D. F., and W. F. Morris. 2010. Demographic compensation and tipping points in climate-induced range shifts. Nature 467:959–962.

Duputié, A., F. Massol, I. Chuine, M. Kirkpatrick, and O. Ronce. 2012. How do genetic correlations affect species range shifts in a changing environment? Ecology Letters 15:251–259.

Ehrlén, J., and Z. Münzbergová. 2009. Timing of flowering: opposed selection on different fitness components and trait covariation. American Naturalist 173:819–830.

Engen, S., R. Lande, and B.-E. Sæther. 2011. Evolution of a plastic quantitative trait in an age-structured population in a fluctuating environment. Evolution 65:2893–2906.

Franks, S. J., J. J. Weber, and S. N. Aitken. 2014. Evolutionary and plastic responses to climate change in terrestrial plant populations. Evolutionary Applications 7:123–139.

Gienapp, P., M. Lof, T. E. Reed, J. McNamara, S. Verhulst, and M. E. Visser. 2013. Predicting demographically sustainable rates of adaptation: can great tit breeding time keep pace with climate change? Philosophical Transactions of the Royal Society B: Biological Sciences 368:20120289.

Gomulkiewicz, R., and D. Houle. 2009. Demographic and genetic constraints on evolution. American Naturalist 174:E218–E229.

Hamilton, W. D. 1966. Moulding of senescence by natural selection. Journal of Theoretical Biology 12:12–45.

Holt, R. D. 1996. Demographic constraints in evolution: towards unifying the evolutionary theories of senescence and niche conservatism. Evolutionary Ecology 10:1–11.

Janeiro, M. J., D. W. Coltman, M. Festa-Bianchet, F. Pelletier, and M. B. Morrissey. 2017. Towards robust evolutionary inference with integral projection models. Journal of Evolutionary Biology 30:270–288.

Kingsolver, J. G., and S. E. Diamond. 2011. Phenotypic selection in natural populations: what limits directional selection? American Naturalist 177:346–357.

Kopp, M., and S. Matuszewski. 2014. Rapid evolution of quantitative traits: theoretical perspectives. Evolutionary Applications 7:169–191.

Kuparinen, A., O. Savolainen, and F. M. Schurr. 2010. Increased mortality can promote evolutionary adaptation of forest trees to climate change. Forest Ecology and Management 259:1003–1008.

Lande, R. 1982. A quantitative genetic theory of life history evolution. Ecology 63:607–615.

Lande, R., and S. Shannon. 1996. The role of genetic variation in adaptation and population persistence in a changing environment. Evolution 50:434–437.

Lynch, M., and W. Gabriel. 1990. Mutation load and the survival of small populations. Evolution 44:1725–1737.

Lynch, M., W. Gabriel, and A. M. Wood. 1991. Adaptive and demographic responses of plankton populations to environmental change. Limnology and Oceanography 36:1301–1312.

Lynch, M., and R. Lande. 1993. Evolution and extinction in response to environmental change. Pages 234–250 *in* P. Kareiva, J. Kingslover, and R. Huey, eds. Biotic interactions and global change. Sinauer, Sunderland, MA.

Marshall, D. J., S. C. Burgess, and T. Connallon. 2016. Global change, life-history complexity and the potential for evolutionary rescue. Evolutionary Applications 9:1189–1201.

Mojica, J. P., and J. K. Kelly. 2010. Viability selection prior to trait expression is an essential component of natural selection. Proceedings of the Royal Society B 277:2945–2950.

Morris, W. F., and D. F. Doak. 2004. Buffering of life histories against environmental stochasticity: accounting for a spurious correlation between the variabilities of vital rates and their contributions to fitness. American Naturalist 163:579–590.

Nunney, L. 2015. Adapting to a changing environment: modeling the interaction of directional selection and plasticity. Journal of Heredity 107:15–24.

Orive, M. E., M. Barfield, C. Fernandez, and R. D. Holt. 2017. Effects of clonal reproduction on evolutionary lag and evolutionary rescue. American Naturalist 190:469–490.

Osmond, M. M., and C. A. Klausmeier. 2017. An evolutionary tipping point in a changing environment. Evolution 71:2930–2941.

Polechová, J., N. Barton, and G. Marion. 2009. Species' range: adaptation in space and time. American Naturalist 174:E186–E204.

Przeslawski, R., M. Byrne, and C. Mellin. 2015. A review and meta-analysis of the effects of multiple abiotic stressors on marine embryos and larvae. Global Change Biology 21:2122–2140.

Reed, T. E., V. Grøtan, S. Jenouvrier, B.-E. Sæther, and M. E. Visser. 2013. Population growth in a wild bird is buffered against phenological mismatch. Science 340:488–491.

Ronce, O., and M. Kirkpatrick. 2001. When sources become sinks: migrational meltdown in heterogeneous habitats. Evolution 55:1520–1531.

Salguero-Gómez, R., O. R. Jones, C. R. Archer, Y. M. Buckley, J. Che-Castaldo, H. Caswell, D. Hodgson, A. Scheuerlein, D. A. Conde, and E. Brinks. 2015. The COMPADRE plant matrix database: an open online repository for plant demography. Journal of Ecology 103:202–218.

Schluter, D., T. D. Price, and L. Rowe. 1991. Conflicting selection pressures and life history trade-offs. Proceedings of the Royal Society B 246:11–17.

Siepielski, A. M., J. D. DiBattista, J. A. Evans, and S. M. Carlson. 2011. Differences in the temporal dynamics of phenotypic selection among fitness components in the wild. Proceedings of the Royal Society B 278:1572–1580.

Siepielski, A. M., M. B. Morrissey, M. Buoro, S. M. Carlson, C. M. Caruso, S. M. Clegg, T. Coulson, J. DiBattista, K. M. Gotanda, and C. D. Francis. 2017. Precipitation drives global variation in natural selection. Science 355:959–962.

Tarwater, C. E., and S. R. Beissinger. 2013. Opposing selection and environmental variation modify optimal timing of breeding. Proceedings of the National Academy of Sciences of the USA 110:15365–15370.

van Mantgem, P. J., and N. L. Stephenson. 2007. Apparent climatically induced increase of tree mortality rates in a temperate forest. Ecology Letters 10:909–916.

Villellas, J., D. F. Doak, M. B. García, and W. F. Morris. 2015. Demographic compensation among populations: what is it, how does it arise and what are its implications? Ecology Letters 18:1139–1152.

Vitasse, Y. 2013. Ontogenic changes rather than difference in temperature cause understory trees to leaf out earlier. New Phytologist 198:149–155.

Wachter, K. W., S. N. Evans, and D. Steinsaltz. 2013. The age-specific force of natural selection and biodemographic walls of death. Proceedings of the National Academy of Sciences of the USA 110:10141–10146.

Wadgymar, S. M., S. C. Daws, and J. T. Anderson. 2017. Integrating viability and fecundity selection to illuminate the adaptive nature of genetic clines. Evolution Letters 1:26–39.

Willi, Y., and A. A. Hoffmann. 2009. Demographic factors and genetic variation influence population persistence under environmental change. Journal of Evolutionary Biology 22:124–133.

Zeineddine, M., and V. A. Jansen. 2009. To age, to die: parity, evolutionary tracking and Cole's paradox. Evolution 63:1498–1507.

References Cited Only in the Online Appendixes

Bontemps, A., F. Lefèvre, H. Davi, and S. Oddou-Muratorio. 2016. In situ marker-based assessment of leaf trait evolutionary potential in a marginal European beech population. Journal of Evolutionary Biology 29:514–527.

Chuine, I., and E. G. Beaubien. 2001. Phenology is a major determinant of tree species range. Ecology Letters 4:500–510.

Harcombe, P. 1987. Tree life tables. Bioscience 37:557–568.

Vitasse, Y., C. François, N. Delpierre, E. Dufrêne, A. Kremer, I. Chuine, and S. Delzon. 2011. Assessing the effects of climate change on the phenology of European temperate trees. Agricultural and Forest Meteorology 151:969–980.

Vitasse, Y., A. Lenz, G. Hoch, and C. Körner. 2014. Earlier leaf-out rather than difference in freezing resistance puts juvenile trees at greater risk of damage than adult trees. Journal of Ecology 102:981–988.

Special Feature Editor: Joseph Travis

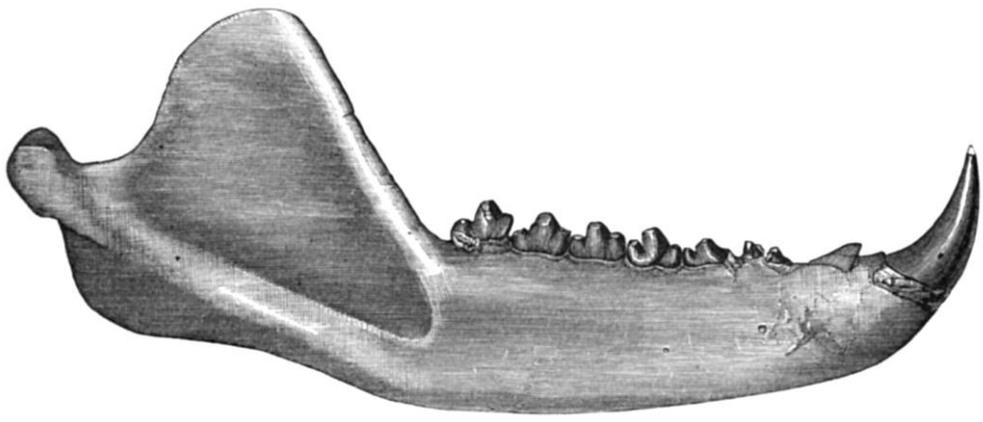

"Present knowledge justifies the generalization that, since the Eocene period, the mammalian fauna of the Northern hemisphere has diminished in the number of its species and genera." Figured: "Mandible of *Mesonyx ossifragus* Cope, from the Wasatch epoch of the Big Horn river, Wyoming." From "The Creodonta" by E. D. Cope (*The American Naturalist*, 1884, 18:255–267).